American Mineralogist, Volume 94, pages 771–776, 2009

Inverse spinel structure of Co-doped gahnite

JASMINKA POPOVIĆ,[1,*] EMILIJA TKALČEC,[2] BISERKA GRŽETA,[1] STANISLAV KURAJICA,[2] AND BORIS RAKVIN[3]

[1]Division of Materials Physics, Ruđer Bošković Institute, P.O. Box 180, HR-10002 Zagreb, Croatia
[2]Faculty of Chemical Engineering and Technology, University of Zagreb, Marulićev trg 19, HR-10000 Zagreb, Croatia
[3]Division of Physical Chemistry, Ruđer Bošković Institute, P.O. Box 180, HR-10002 Zagreb, Croatia

ABSTRACT

Powder $ZnAl_2O_4$ (gahnite) samples doped with 0–100 at% Co were obtained by a sol-gel technique. X-ray powder diffraction was used to characterize the samples. Gahnite samples are cubic with the normal spinel structure, space group $Fd\bar{3}m$. Cobalt doping caused a nonuniform increase of unit-cell parameter. The structure of the gahnite samples was refined by the Rietveld method. The location of Co^{2+} was determined by EPR spectroscopy. Cobalt doping of gahnite induces the inverse spinel structure at only 4 at% Co, and the inversion parameter increases with Co^{2+} doping level. Metal-oxide distances in the $(Al,Co)O_6$ octahedra dominantly influence the unit-cell parameter of Co-doped gahnite.

Keywords: Co-doped gahnite, spinel structure, X-ray powder diffraction, Rietveld method

INTRODUCTION

Zinc aluminate ($ZnAl_2O_4$), known by the mineral name gahnite, is a semiconductor with a wide energy band gap of ~3.9 eV. It is transparent for wavelengths greater than 320 nm, but shows large absorbance in the UV region. Due to its properties, zinc aluminate can be used for various ultraviolet photoelectronic devices (Sampath and Cordaro 1998; Omata et al. 1994). Furthermore, it is used as a catalytic material in various chemical and petrochemical industries (El-Nabarway et al. 1995; Valenzuela et al. 1997), and also as a ceramic material (Roesky et al. 1990). When doped with Co^{2+}, Mn^{2+}, and rare earth cations, it exhibits luminescence and can be used as a cathodoluminescent material (Müller 2002). Zinc aluminate possesses a normal spinel structure (O'Neill and Dollase 1994; Sickafus et al. 1999) that can be described with the general formula AB_2X_4. Spinels crystallize in the cubic system, in the space group $Fd\bar{3}m$. The unit cell contains 32 X^{2-} anions in a face-centered cubic packing (fcc). Inside the anion lattice, cations have 32 octahedral and 64 tetrahedral interstices available. In normal spinel structures, 1/8 of the tetrahedral interstices are occupied by divalent cations A^{2+}, while 1/2 of the octahedral interstices are occupied by trivalent cations B^{3+}. The conventional choices for the unit-cell origin in spinel are either on the A-site cation ($\bar{4}3m$ symmetry) or on the octahedral vacancy ($\bar{3}m$ symmetry) as reported by Sickafus et al. (1999). Regardless of origin setting, anions are always located on position 32*e*. The coordinates of the anions at equipoint 32*e* are not special: they vary according to a single parameter, the anion positional parameter, *u*. For a perfect fcc anion arrangement, $u_{(\bar{4}3m)} = 3/8$ and $u_{(\bar{3}m)} = 1/4$, respectively. Depending on the A/B cation radii ratio, the anion sublattice expands or contracts by varying *u* until the volume of the tetrahedral and octahedral voids match the radii of constituent cations. As *u* increases from its ideal value, anions move along the [111] direction away from the tetrahedraly coordinated cations, which increases the volume of each tetrahedral site, while octahedral sites become correspondingly smaller. Spinels can demonstrate some degree of cation disorder, which Verwey and Heilmann (1947) described by introducing an inversion parameter, δ. This parameter is defined as a fraction of trivalent metal cation B^{3+} on tetrahedral cation sites (or a fraction of divalent metal cations A^{2+} on octahedral cation sites). In this way, the structural formula for spinels may be written as $^{IV}[A_{1-\delta}B_\delta]\ ^{VI}[B_{2-\delta}A_\delta]\ X_4$. Some of the principal factors that influence cation inversion are temperature, cation radii, cation charge, electrostatic contribution to the lattice energy, and crystal-field effects.

O'Neill and Dollase (1994) performed a detailed structural study of zinc aluminate powder samples annealed in the temperature range from 700 to 1400 °C and then rapidly quenched in water. It was found that the unit-cell parameter *a* slightly increased and oxygen positional parameter *u* slightly decreased in annealing, reflecting a small increase of inversion parameter δ (0.01–0.06 depending on the temperature of annealing). Also, the unit-cell parameter *a* of the powder sample annealed at 1200 °C was found to be equal (within the standard deviation) to the unit-cell parameter of single-crystal sample annealed at the same temperature. From these investigations, it could be concluded that gahnite generally possesses a normal spinel structure regardless of temperature.

In contrast to the structure of zinc aluminate, the structure of cobalt aluminate ($CoAl_2O_4$) displays a pronounced inversion even at room temperature (δ = 0.155) as found by Toriumi et al. (1978). Nakatsuka et al. (2003) performed a structural study by means of X-ray powder diffraction and Rietveld structure refinement of $CoAl_2O_4$ samples, which were annealed at various

* E-mail: jpopovic@irb.hr

temperatures between 700 to 1350 °C and then rapidly quenched in water. They noticed that the unit-cell parameter *a* increased and the oxygen positional parameter *u* decreased with increasing annealing temperature up to 1250 °C, as a consequence of the increase in structure inversion with temperature. The inversion parameter δ reached a maximum value of 0.23 at 1250 °C. The decrease in the inversion parameter value for the sample annealed at 1350 °C was explained by the authors as a possible redistribution between the ^{IV}A and ^{VI}B site occupation during the quenching process of the annealed samples.

To the best of our knowledge, structural studies of Co-doped $ZnAl_2O_4$ are not abundant in the literature. Duan et al. (2005) investigated microstructure and spectroscopic properties of Co^{2+}:$ZnAl_2O_4$/SiO_2 nanocomposite glasses containing nanocrystalline Co-doped $ZnAl_2O_4$ dispersed in a silica glass matrix. The samples were prepared by the sol-gel technique. The gels were of composition $89SiO_2$-$6Al_2O_3$-5ZnO-xCoO (x = 0.2, 0.4, 0.6, 0.8, 1). The absorption spectra of the prepared samples consisted of two bands: a strong absorption band centered at 590 nm and a broad absorption band centered at 1400 nm. The observed visible and near-infrared absorption bands are characteristic of tetrahedrally coordinated Co^{2+} cations. The absorbance of the spectra increased with an increase in the Co content indicating pronounced incorporation of Co^{2+} on tetrahedral sites in the $ZnAl_2O_4$ structure. The lattice constant of Co-doped $ZnAl_2O_4$ increased with an increase in Co-doping level, which the authors explained by a simple Co^{2+} substitution for Zn^{2+}, obviously disregarding the fact that the mentioned substitution would lead to a decrease of unit-cell parameter (cation radii for tetrahedral Zn^{2+} and Co^{2+} being 0.60 and 0.58 Å, respectively).

The present paper reports the preparation of Co-doped gahnite samples by a sol-gel technique and their structural characterization. The structural location of Co^{2+} cations has been proposed on the basis of EPR spectroscopy and the Rietveld structure refinement of XRD powder data.

Experimental methods

Sample preparation

Powder samples of zinc aluminate doped with 0, 4, 8, 12, 25, 40, 50, 60, 75, 90, and 100 at% Co (substituted for Zn) were prepared by a sol-gel technique. Aluminum-*sec*-butoxide, zinc nitrate hexahydrate [$Zn(NO_3)_2 \cdot 6H_2O$], and cobalt nitrate hexahydrate [$Co(NO_3)_3 \cdot 6H_2O$] were dissolved in 2-butanole by vigorous stirring. Prepared gels were dried at room temperature during few days, then additionally annealed at 800 °C for 2 h and slowly cooled to RT in the furnace. The prepared samples were denoted as S0 to S10 (Table 1). Sample S0 was white, while other samples were blue, from light blue (S1) to dark blue (S10).

Table 1. Refined unit-cell parameter *a* for samples S0–S10

Sample	Co content (at%)	R_p	R_{wp}	*a* (Å)
S0	0	0.048	0.063	8.0854(3)
S1	4	0.036	0.057	8.0863(5)
S2	8	0.035	0.052	8.0883(4)
S3	12	0.039	0.056	8.0897(4)
S4	25	0.039	0.059	8.0914(3)
S5	40	0.033	0.050	8.0924(4)
S6	50	0.034	0.050	8.0928(5)
S7	60	0.040	0.056	8.0931(7)
S8	75	0.038	0.053	8.0945(6)
S9	90	0.032	0.049	8.0973(6)
S10	100	0.030	0.051	8.1005(5)

Note: R_p and R_{wp} are the discrepancy factors that characterize a quality of the fit (Young et al. 1982).

Methods

Structural changes due to Co incorporation in the zinc aluminate lattice were studied by X-ray diffraction (XRD) at room temperature using a Philips MPD 1880 counter diffractometer with Cu*K*α radiation. Two data sets were collected for each prepared gahnite sample: (1) XRD pattern of the sample mixed with a standard reference material, silicon powder (Koch-Light Lab. Ltd., 99.999% purity), scanned in steps of 0.02 °(2θ) in the 2θ range from 10 to 100° with fixed counting time of 7 s per step, for the purpose of precise determination of unit-cell parameters; and (2) XRD pattern of the pure sample scanned in the 2θ range from 10 to 140° also in steps of 0.02 °(2θ) and with fixed counting time of 7 s per step, for the purpose of the Rietveld structure refinement (Rietveld 1969). Precise determination of the unit-cell parameter *a* of prepared samples was performed by the method proposed by Toraya (1993). Bragg angle positions (2θ) of several diffraction lines of the examined sample and three diffraction lines of silicon were determined by individual profile-fitting method (program PROFIT: Toraya 1986) and taken as input data for the program UNITCELL (Toraya 1993). Initial unit-cell parameters were refined by the whole-powder-pattern decomposition method (program WPPF: Toraya 1986) using the split-type pseudo-Voigt profile function and the polynomial background model. Crystal structures of the prepared samples were refined by the Rietveld method with the program X'Pert HighScore Plus, version 2.1 (PANalytical 2004), using a pseudo-Voigt profile function and also the polynomial background model. Isotropic vibration modes were assumed for all atoms.

EPR spectroscopy was performed for examining the Co position in the Co-doped gahnite structure. Investigation was carried out with standard X-band EPR spectrometer Bruker Elexys FT/CW 580 at low temperatures (10 to 70 K). All spectra were obtained with the magnetic field amplitude of 0.3 mT at 100 KHz. The microwave power used was about 0.6 mW and spectra were detected at the first harmonic of the modulation frequency.

Results and discussion

XRD characterization of samples

XRD patterns of the prepared samples S0–S10 indicated that all prepared gahnite samples had a characteristic cubic spinel structure. No impurities were detected in the samples. Refined values of unit-cell parameter *a* for prepared gahnite samples are listed in Table 1. The unit-cell parameter of gahnite increased with Co-doping level. A pronounced increase of the unit-cell parameter was noticed for gahnite samples doped with 0–25 and 75–100 at% Co in comparison with those containing 25–75 at% Co, as presented in Figure 1. With Co doping, the decrease of unit-cell parameter should be expected considering that ionic radius of 4-coordinated Co^{2+} is smaller than that of 4-coordinated Zn^{2+}. However, the opposite trend was noticed. The observed lattice expansion is an indication of a considerable level of structure inversion in gahnite due to Co doping. That means that only a

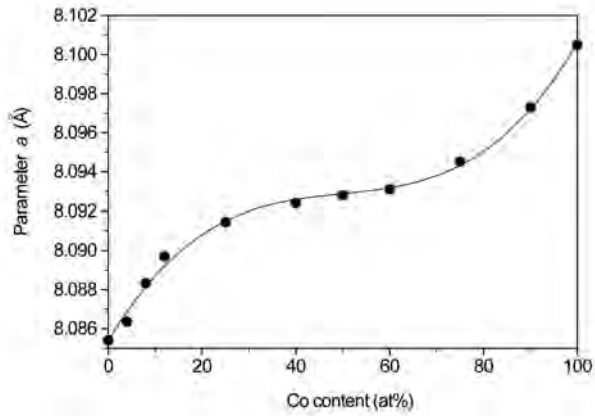

Figure 1. Relationship between unit-cell parameter *a* of Co-doped gahnite and Co^{2+} content.

part of Co^{2+} substitutes for Zn^{2+} on tetrahedral cation sites, and the remaining Co^{2+} substitutes for Al^{3+} on octahedral cation sites in the $ZnAl_2O_4$ lattice, causing the increase of unit-cell parameter (ionic radii of octahedrally coordinated Al^{3+} and high-spin Co^{2+} being 0.535 and 0.745 Å, respectively). A nonuniform increase of unit-cell parameter with increase of Co-doping level (Fig. 1) suggests a nonuniform Co^{2+} substitution mechanism.

EPR spectroscopy

EPR spectra of the samples S1, S2, and S3 collected at 10 K are shown in Figure 2. The spectra display a typical distorted axial pattern for high-spin Co^{2+} centers with three major resonance features. These spectra are in agreement with expectation for molecules with $S = 3/2$ subjected to zero-field splitting where only the (±1/2) Kramer's doublet, identified from the effective g values, is resonant (Weil et al. 1994). An additional multiple splitting with low intensity is incorporated in the broad low-field resonance signal, as clearly seen for the sample with lowest concentration of Co^{2+} centers. The amount of splitting between these lines is 11.5 mT (insert in Fig. 2) and corresponds to eight lines of hyperfine splitting of ^{59}Co nuclear spin (I = 7/2). The effective g value of this spectral component is $g = 7.79$. To elucidate a possible character of the obtained EPR spectra, the additional spectra for sample S1 were taken at 35 and 70 K (Fig. 3). With the increase in temperature, the intensity of EPR components decreased. At 70 K, the spectrum became dominated by two broad components at $g = 5.30$ and $g = 2.0$ indicating that these components had a slightly slower relaxation than other spectrum components seen at lower temperatures. This evidently showed that the EPR spectra of Co-doped gahnite have the composite character. The components can be identified as contributions to the spectra from Co^{2+} cations in more than one local environment. Indeed, in accord with the previous EPR studies (Sellin et al. 1983) the values $g = 7.79$, $g = 2.22$, and $g = 1.84$ and hyperfine splitting are consistent with Co^{2+} center on distorted octahedral cation site. On the other hand, the spectral components at $g = 5.30$ and $g = 2.0$ are characteristic of Co^{2+} centered on the tetrahedral cation site (Pountney and Vašak 1992). Based on these results, a general formula for Co-doped gahnite can be written as $^{IV}[Zn_{1-x}Co_{x-\delta}Al_{\delta}]\ ^{VI}[Al_{2-\delta}Co_{\delta}]\ O_4$, where x represents the level of incorporated Co^{2+} cations in the gahnite structure, and δ is the inversion parameter of the spinel structure.

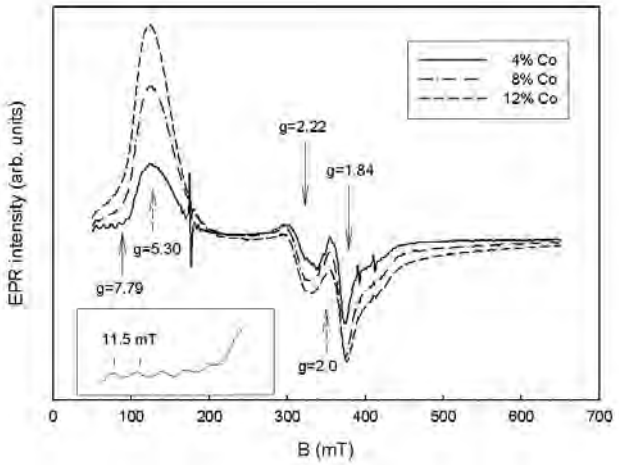

FIGURE 2. EPR spectra of Co-doped samples S1, S2, and S3 (containing 4, 8, and 12 at% Co, respectively) taken at 10 K. Solid arrows denote g values for Co^{2+} cation on the octahedral site, while dashed arrows denote g values for tetrahedrally coordinated Co^{2+} cation. The small sharp peaks near 180, 390, and 405 mT correspond to the resonance cavity signals.

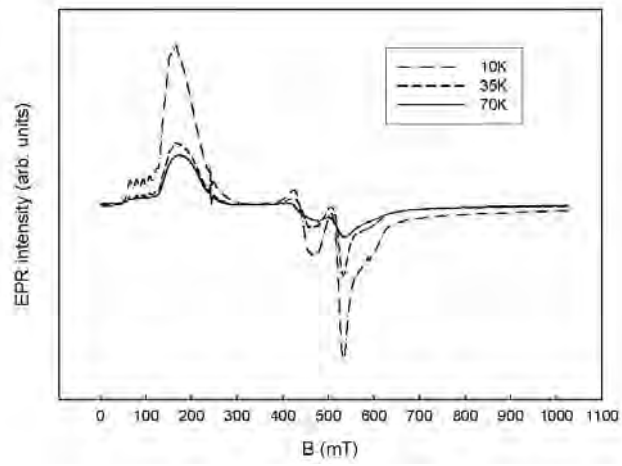

FIGURE 3. EPR spectra of sample S1 taken at 10, 35, and 70 K.

Rietveld structure refinement

The crystal structures of the samples S0, S1, S2, S3, S4, S6, S8, and S10 were refined by the Rietveld method. The structure of undoped gahnite reported by O'Neill and Dollase (1994) was used as the starting structure model for our undoped gahnite (sample S0). For the Co-doped samples, a gahnite structure model

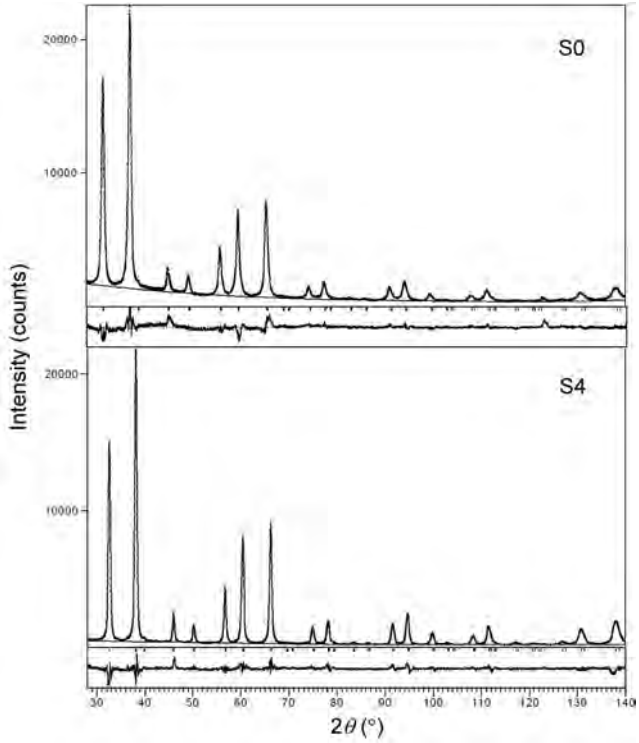

FIGURE 4. Result of the Rietveld refinement for samples S0 and S4.

TABLE 2. Results of Rietveld refinements: Structural parameters and their standard deviations for samples S0, S1, S2, S3, S4, S6, S8, and S10

Sample	δ	R_{wp}	Atom site	Wyck. position	Occupancy	$x = y = z$	B_{iso} (Å^2)
S0	0	0.059	^{IV}A	8*a*	1 Zn	0.125	0.97(2)
			^{VI}B	16*d*	1 Al	0.5	0.29(3)
			O	32*e*	1 O	0.2644(1)*	0.53(5)
S1	0.037(4)	0.068	^{IV}A	8*a*	0.003 Co + 0.96 Zn + 0.037 Al	0.125	0.90(1)
			^{VI}B	16*d*	0.0185 Co + 0.9815 Al	0.5	0.45(2)
			O	32*e*	1 O	0.2640(1)	0.48(3)
S2	0.051(3)	0.072	^{IV}A	8*a*	0.029 Co + 0.92 Zn + 0.051 Al	0.125	0.90(2)
			^{VI}B	16*d*	0.0255 Co + 0.9745 Al	0.5	0.47(2)
			O	32*e*	1 O	0.2636(1)	0.51(3)
S3	0.055(4)	0.057	^{IV}A	8*a*	0.065 Co + 0.88 Zn + 0.055 Al	0.125	0.90(2)
			^{VI}B	16*d*	0.0275 Co + 0.9725 Al	0.5	0.44(1)
			O	32*e*	1 O	0.2634(9)	0.43(3)
S4	0.070(3)	0.054	^{IV}A	8*a*	0.18 Co + 0.75 Zn + 0.07 Al	0.125	1.06(6)
			^{VI}B	16*d*	0.035 Co + 0.965 Al	0.5	0.48(1)
			O	32*e*	1 O	0.2631(8)	0.55(2)
S6	0.095(4)	0.056	^{IV}A	8*a*	0.405 Co + 0.5 Zn + 0.095 Al	0.125	0.94(3)
			^{VI}B	16*d*	0.0475 Co+0.9525 Al	0.5	0.64(2)
			O	32*e*	1 O	0.2629(1)	0.63(3)
S8	0.150(4)	0.059	^{IV}A	8*a*	0.6 Co + 0.25 Zn + 0.15 Al	0.125	0.58(2)
			^{VI}B	16*d*	0.075 Co + 0.925 Al	0.5	0.68(2)
			O	32*e*	1 O	0.2625(1)	0.67(3)
S10	0.248(5)	0.061	^{IV}A	8a	0.752 Co + 0.248 Al	0.125	0.97(7)
			^{VI}B	16d	0.124 Co + 0.876 Al	0.5	0.37(2)
			O	32e	1 O	0.2613(1)	0.72(5)

* Coordinate of oxygen at 32*e* is known as oxygen positional parameter *u*.

was used that had a portion of tetrahedrally coordinated Zn^{2+} and a portion of octahedrally coordinated Al^{3+} ions substituted by Co^{2+} ions. In the structure refinement procedure, the site occupancy parameters for cations (Zn^{2+}, Co^{2+}, and Al^{3+} on the tetrahedral site and Al^{3+} and Co^{2+} on the octahedral site) were determined indirectly, namely by varying the inversion parameter δ under the constrain that maintained the chemical composition of the sample. Isotropic temperature factors (B_{iso}) for cations sharing the same cation site were constrained to change identically during the Rietveld refinement.

The observed and calculated powder patterns for the samples S0 and S4 are presented in Figure 4. Refined structural parameters are given in Table 2. The refinement confirmed the spinel-type structure of the samples. However, only sample S0 possesses the normal spinel structure. Crystal structures of other samples display a nonzero inversion parameter δ in the range between 0.054 (for S1) and 0.248 (for S10). The inversion parameter increased with increasing Co content in gahnite as seen in Figure 5. The value of the inversion parameter for pure $CoAl_2O_4$ (sample S10) is consistent with results obtained by Nakatsuka et al. (2003). The oxygen positional parameter *u* decreased with the increase of Co content in gahnite indicating a decrease of the tetrahedral site volume and expansion of the octahedral site volume with Co doping. This is a consequence of both Zn^{2+} substitution by smaller $^{IV}Co^{2+}$ cations on the tetrahedral site and Al^{3+} substitution by larger $^{VI}Co^{2+}$ cations on the octahedral site. Table 3 lists metal-oxygen distances in tetrahedra and octahedra for gahnite samples. In Figure 6, it can be seen that metal-oxygen distances in tetrahedra decrease almost linearly with the increase of inversion parameter, while metal-oxygen distances in octahedra simultane-

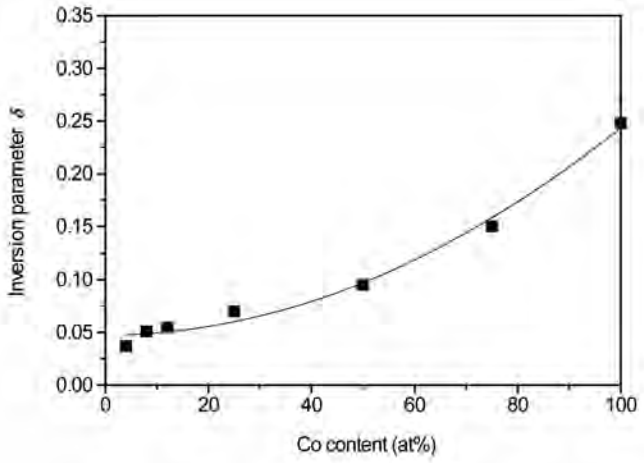

FIGURE 5. Variation of inversion parameter δ with Co content in gahnite samples.

TABLE 3. Metal-oxygen distances (Å) in structural tetrahedra and octahedra of gahnite samples

Sample	Co content (at%)	Inversion parameter δ	Interatomic distances M-O (Å)	
			tetrahedra	octahedra
S0	0	0	1.953	1.913
S1	4	0.037	1.948	1.917
S2	8	0.051	1.943	1.920
S3	12	0.054	1.940	1.921
S4	25	0.070	1.937	1.925
S6	50	0.095	1.932	1.926
S8	75	0.150	1.929	1.929
S10	100	0.248	1.914	1.939

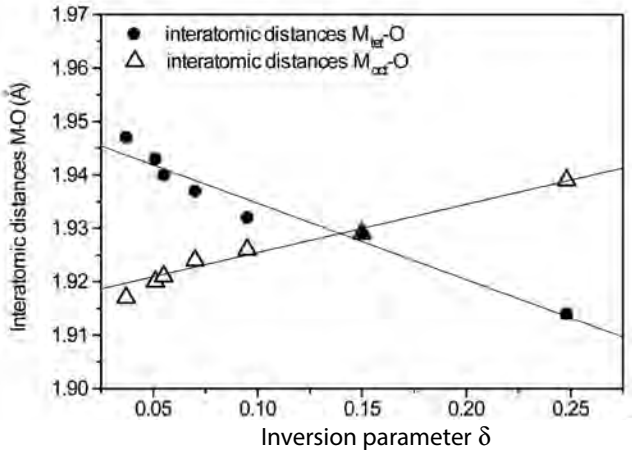

FIGURE 6. Metal-oxygen distances in tetrahedra and octahedra of gahnite with inversion parameter δ.

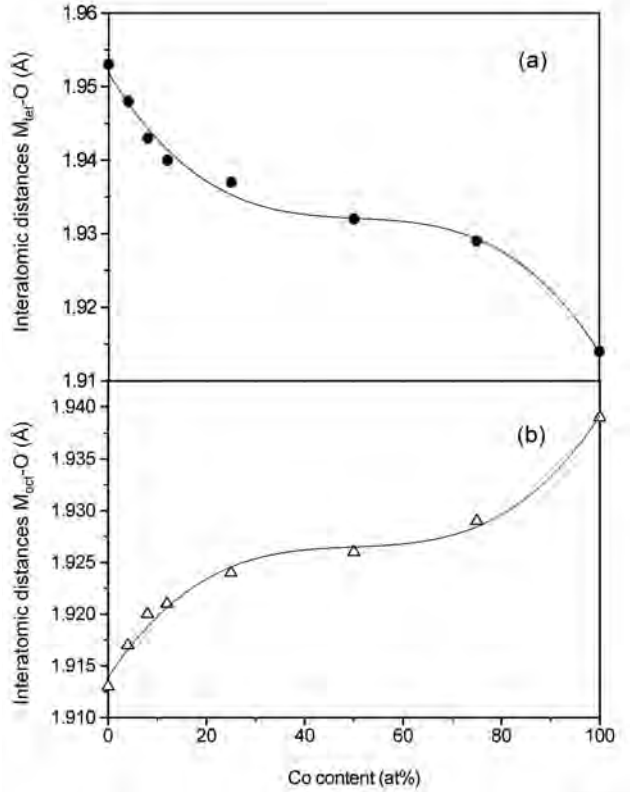

FIGURE 7. Metal-oxygen distances in (**a**) structural tetrahedra and (**b**) structural octahedra as a function of Co content in gahnite.

ously increase almost linearly. The same type of dependence on inversion parameter of the metal-oxygen distances was noted for $CoAl_2O_4$ samples that suffered an increase of structure inversion on annealing (Nakatsuka et al. 2003).

Changes in metal-oxygen distances in structural tetrahedra and octahedra of gahnite as a function of Co-doping level are shown in Figure 7. Metal-oxygen distances in tetrahedra decrease with doping level (Fig. 7a), while metal-oxygen distances in octahedra increase (Fig. 7b). It is obvious that the change of metal-oxygen distance in the structural octahedra of gahnite

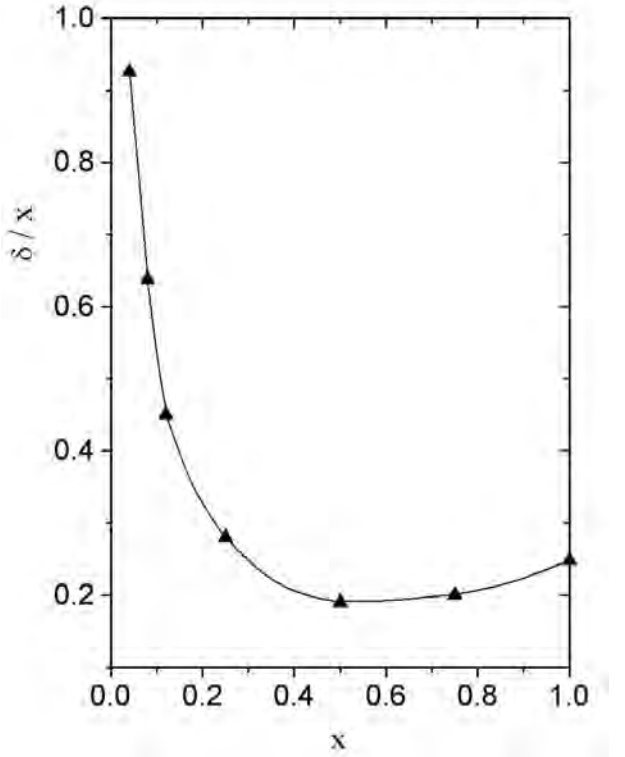

FIGURE 8. Dependence of Co content of octahedra on total Co content in gahnite.

caused by Co doping (Fig. 7b) has the same trend as the change of unit-cell parameter of gahnite (Fig. 1). This is quite understandable since the metal-oxygen bonds in octahedra, M_{oct}-O, are almost parallel to the [100], [010], and [001] axes. The change of interatomic distances in tetrahedra has much smaller impact on the unit-cell parameter of gahnite because M_{tetr}-O bonds make an angle of ~53° with the [100], [010], and [001] axes. Besides, in the spinel-type structure there are twice as many structural octahedra as tetrahedra.

The nonuniform increase in the unit-cell parameter of gahnite with increasing Co content may be explained by the results of the Rietveld structure refinements as follows. In doping, a portion of the Co content occupies tetrahedral sites of the gahnite structure (substituting for Zn), and a portion occupies octahedral sites (substituting for Al). The portion of Co that occupies the octahedral sites is given by the ratio of inversion parameter (δ) and total Co content (x), namely δ/x. Figure 8 presents the dependence of δ/x on Co content, x, in doped gahnite samples. For the examined doped gahnite samples, δ/x has a minimum at Co content x = 0.5, as seen in Figure 8. According to this, at a low Co-doping level the portion of Co on octahedral sites is a large part of total Co content (almost 93% of total Co content at x = 0.04). This induces a pronounced increase of unit-cell parameter for low doping levels. In further doping, the portion of Co on octahedral sites decreases until it reaches 19% of total Co content for doping level x = 0.5, causing a slower increase of unit-cell parameter with saturation at x = 0.5. After the doping level of 0.5, the portion of Co on octahedral sites increases, which causes a renewed faster increase of unit-cell parameter at x > 0.5.

ACKNOWLEDGMENT

Financial support from the Ministry of Science, Education, and Sports of Republic of Croatia is gratefully acknowledged.

REFERENCES CITED

Duan, X.L., Yuan, D.R., Cheng, X.F., Sun, H.Q., Sun, Z.H., Wang, X.Q., Wang, Z.M., Xu, D., and Lv, M.K. (2005) Microstructure and properties of Co^{2+}: $ZnAl_2O_4/SiO_2$ nanocomposite glasses prepared by Sol–Gel method. Journal of the American Ceramic Society, 88, 399–403.

El-Nabarway, T., Attia, A.A., and Alaya, M.N. (1995) Effect of thermal treatment on the structural, textural and catalytic properties of the $ZnO\text{-}Al_2O_3$ system. Materials Letters, 25, 319–325.

Müller, G. (2002) Electroluminescence II, Semiconductors and Semimetals, p. 60–68. Academic Press, New York.

Nakatsuka, A., Ikeda, Y., Yamasaki, Y., Nakayama, N., and Mizota, T. (2003) Cation distribution and bond lengths in $CoAl_2O_4$ spinel. Solid State Communications, 128, 85–90.

Omata, T., Ueda, K., Ueda, N., and Kawazoe, H. (1994) New ultraviolet-transport electroconductive oxide, $ZnGa_2O_4$ spinel. Applied Physical Letters, 64, 1077–1079.

O'Neill, H.St.C. and Dollase, W.A. (1994) Crystal structures and cation distributions in simple spinels from powder XRD structural refinements: $MgCr_2O_4$, $ZnCr_2O_4$, Fe_3O_4, and the temperature dependence of the cation distribution in $ZnAl_2O_4$. Physics and Chemistry of Minerals, 20, 541–555.

PANalytical (2004) X'Pert HighScore Plus Program, version 2.1. Almelo, Netherlands.

Pountney, D. and Vašak, M. (1992) Spectroscopic studies on metal distribution in Co(II)/Zn(II) mixed-metal clusters in rabbit liver metallothionein 2. European Journal of Biochemistry, 209, 335–341.

Rietveld, H.M. (1969) Line profiles of neutron powder-diffraction peaks for structure refinement. Journal of Applied Crystallography, 2, 65–71.

Roesky, R., Weiguny, J., Bestgen, H., and Durgerdissen, U. (1990) An improved synthesis method for indenes and styrenes by use of a ZnO/Al_2O_3 spinel catalyst. Applied Catalyst A: General, 176, 213–220.

Sampath, S.K. and Cordaro, J.F. (1998) Optical properties of zinc aluminate, zinc gallate, and zinc aluminogallate spinels. Journal of the American Ceramic Society, 81, 649–652.

Sellin, S., Eriksson, L.E.G., Aronsson, A., and Mannervik, B. (1983) Octahedral metal coordination in the active site of glyoxalase I as evidenced by the properties of Co(II)-glyoxalase. Journal of the Biological Chemistry, 258, 2091–2093.

Sickafus, K.E. and Wills, J.M. (1999) The structure of spinel. Journal of the American Ceramic Society, 82, 3279–3292.

Toraya, H. (1986) Whole-powder-pattern fitting without reference to a structural model: Application to X-ray powder diffraction data. Journal of Applied Crystallography, 19, 440–447.

——— (1993) The determination of unit-cell parameters from Bragg reflection data using a standard reference material but without a calibration curve. Journal of Applied Crystallography, 26, 583–590.

Toriumi, K., Ozima, M., Akaogi, M., and Saito, Y. (1978) Electron-density distribution in crystals of $CoAl_2O_4$. Acta Crystallographica, B34, 1093–1096.

Valenzuela, M.A., Jacobs, J.P., Bosch, P., Reijne, S., Zapata, B., and Brongersma, H.H. (1997) The influence of the preparation method on the surface structure of $ZnAl_2O_4$. Applied Catalyst A, 148, 315–324.

Verwey, E.J.W. and Heilmann, E.L. (1947) Physical properties and cation arrangement of oxides with spinel structures. Journal of Chemistry and Physics, 15, 174–180.

Weil, J.A., Bolton, J.R., and Wertz, J.E. (1994) Electron Paramagnetic Resonance: Elementary Theory and Practical Applications, p. 213–232. Wiley, New York.

Young, R.A., Prince, E., and Sparks, R.A. (1982) Suggested guidelines for the publication of Rietveld analyses and pattern decomposition studies. Journal of Applied Crystallography, 15, 357–359.

MANUSCRIPT RECEIVED DECEMBER 16, 2008
MANUSCRIPT ACCEPTED FEBRUARY 3, 2009
MANUSCRIPT HANDLED BY ARTEM OGANOV